Molecular Crystals and Liquid Crystals

ISSN: 1542-1406 (Print) 1563-5287 (Online) Journal homepage: http://www.tandfonline.com/loi/gmcl20

Growth of Dual DLC and Icosahedral Boron Carbide Nano-Crystals by HFCVD

M. Ghoranneviss, A. Salar Elahi & M. Dadashbaba

To cite this article: M. Ghoranneviss, A. Salar Elahi & M. Dadashbaba (2015) Growth of Dual DLC and Icosahedral Boron Carbide Nano-Crystals by HFCVD, Molecular Crystals and Liquid Crystals, 608:1, 103-115, DOI: 10.1080/15421406.2014.949767

To link to this article: http://dx.doi.org/10.1080/15421406.2014.949767

Published online: 03 Mar 2015.

Mol. Cryst. Liq. Cryst., Vol. 608: pp. 103–115, 2015

ISSN: 1542-1406 print/1563-5287 online
DOI: 10.1080/15421406.2014.949767

Growth of Dual DLC and Icosahedral Boron Carbide Nano-Crystals by HFCVD

M. GHORANNEVISS, A. SALAR ELAHI,*
AND M. DADASHBABA

Plasma Physics Research Center, Science and Research Branch, Islamic Azad University, Tehran, Iran

Carbon nano-structures were doped by boron atoms to synthesize icosahedral boron carbide using Hot Filament Chemical Vapor Deposition method. Raman spectroscopy revealed two broad peaks centered on 1,334 and 1,573 cm^{-1}, the origin of which is sp^3 hybrid of diamond (D-band) and sp^2 hybrid of graphite (G-band), respectively. These peaks stem from aromatic compounds with sp^2 hybrid, demonstrating a local collection of amorphous $B_{13}C_2$ on the substrate surface. Furthermore, D and G peaks are illustrative of more damage inside the structure. X-ray diffraction patterns indicated significant peaks assigned to icosahedral ($B_{13}C_2$) structures in planes (012), (021), and (024). Debye–Scherrer calculation showed that, the crystal size of the products was in range of 5–80 nm. Additionally, the graphite grain size was evaluated by Tuinstra–Koenig formula at a 42–73 nm interval. The decrease observed in the intensity of G and D peaks may stem from disrupting the vibrational behavior of the film and diminution of polarizability in the molecules of the lattice. One of the factors inducing the decrease of polarizability the promotion of is a great fraction of δ bonds between B-C atoms. Scanning electron microscopy results showed cauliflowers morphology for the nanostructures.

Keywords Boron carbide; cauliflowers; HFCVD; icosahedral; smooth

1. Introduction

Diamond-like Carbon (DLC) is an amorphous carbon material made of random networks of sp^3 and sp^2 hybrid bonds. DLC material with high sp^3 content has similar properties as single crystal or polycrystalline diamond. They are hard, electrically insulating, chemically inert, very good heat conductors, that they show high electron and hole mobility, negative electron affinity, high breakdown field, light weight, large band gaps (>2 eV), and a high index of refraction ($n>2$). Owing to these properties, DLCs are extensively used in diverse fields such as wear coatings, microelectronics, microtribology, and biomedical technology. However, their insulating properties and wide band gap lead to limitation of their applications in electronics (unless the charge carriers incorporated into them [1–5]). Furthermore, by various boron to carbon stoichiometry, the ratio higher than 2, are known as boron carbides.

*Address correspondence to A. Salar Elahi, Plasma Physics Research Center, Tehran Science and Research Branch, Islamic Azad University, Tehran, Iran. E-mail: Salari_phy@yahoo.com

Color versions of one or more of the figures in the article can be found online at www.tandfonline.com/gmcl.

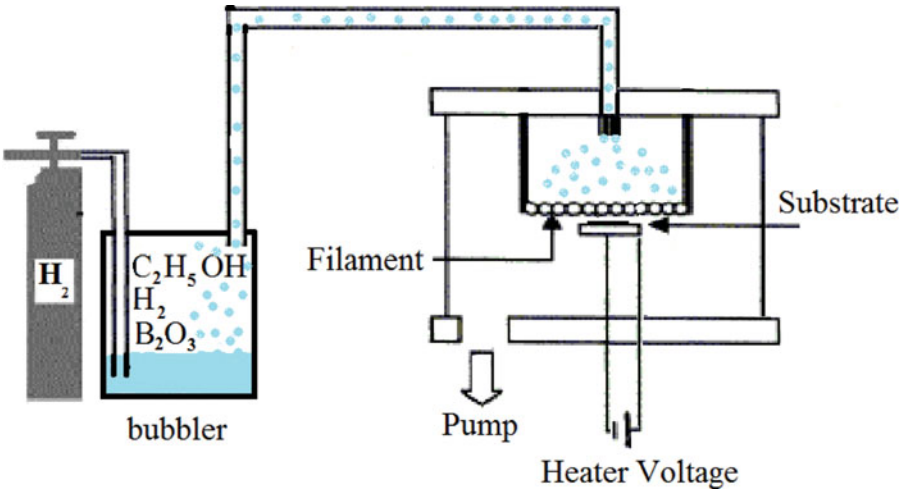

Figure 1. Schematic of HFCVD used in experiment.

Boron carbide exists as a stable single phase compound in a large homogeneity range from 8% up to 20% C concentrations [6]. Boron atom suppresses the formation of sp^2 graphitic clusters and increases both the sp^3 bonding and the hydrogen content in the DLC films [7]. Consequently, the electrical conductivity of the film is a complicated function of the combined effects of the boron-doping level, the grain boundaries, and the impurities. As the grain size in the films becomes smaller, i.e., from Microcrystalline Diamond (MCD) to Nanocrystalline Diamond (NCD), the relative importance of these grain boundaries increases [8, 9]. $B_{13}C_2$ is an attractive hard coating for a variety of applications interestingly [9]. Its high melting point, high modulus, large neutron capture section, low density, chemical inertness, outstanding thermal, and electrical properties make boron carbide a strong candidate for high technology applications [10–14]. Recently, boron-doped diamond or DLC films have been prepared by an assortment of methods including: microwave plasma CVD, plasma-enhanced CVD, photochemical vapor deposition (photo-CVD), DC saddle-field glow-discharge deposition, pulsed laser deposition (PLD), and plasma immersion ion processing [15]. The aim of this research is to present experimental results on the synthesis of DLC and $B_{13}C_2$, nanostructure, chemical composition, deposition rate using HFCVD, and to discuss the influence of boron content on the surface morphology, crystallographic structure of the deposited films.

2. Experimental Details

B-doped DLC films were synthesized with an HFCVD method. The DLC films with different boron-doping levels were produced using solutions with varying boron (B) concentrations, i.e., 0.00626, 0.0125, 0.025, and 0.05 molars (or 0.37×10^1, 7.5×10^{13}, 150×10^{13}, and 3011×10^{13} ppm). The growth process was triggered upon introducing hydrogen gas (H_2) passing through ethanol as B_2O_3 solution in various concentrations in ethanol, as well as boron and carbon source into the chamber. A pure hydrogen gas flow rate of approximately 100 sccm regulated by precision mass flow meter and a total pressure of 15 Torr were maintained throughout the experiment as shown schematically in Fig. 1. The

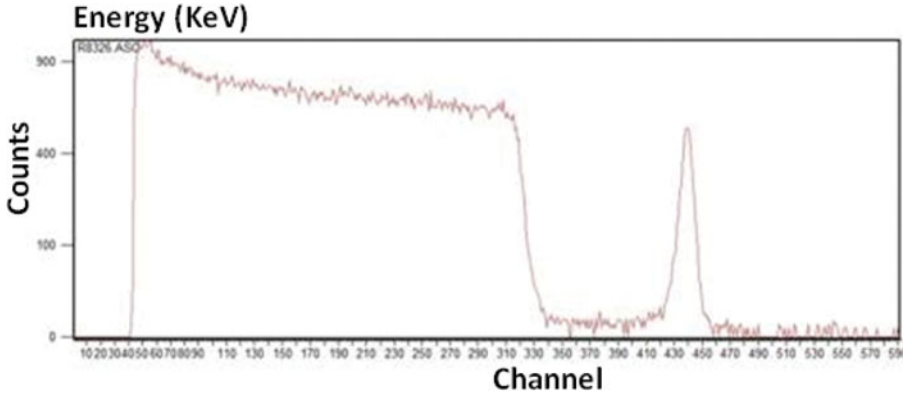

Figure 2. Rutherford back scattering (RBS) show thickness Fe layer deposited on silicon 13 nm.

substrate temperature was 500°C measured by a thermocouple mounted on the substrate surface. Initially, a P-type silicon wafer (100) was cut in 1 × 1 cm^2 pieces and then ultrasonically cleaned in acetone, ethanol, and deionized water, respectively, each for 10 min. Subsequently, Fe films for has been high surface reactivity and absorptivity were sputtered by DC-Magnetron Sputtering with 13 nm thickness measured by Rutherford Back Scattering technique as shown in Fig. 2. Substrates were then placed on the sample platform with a distance of 1 cm between Si substrate and the hot-filament. Prior to synthesis, etching was performed in H_2 ambient for 10 min. Figure 3 illustrates surface roughness before and after etching 0.8 and 26.20 nm, respectively.

The deposition duration of all samples was kept at 30 min in this research. For investigating the surface morphology of the as-grown boron-doped DLC films, a field emission scanning electron microscope (FE-SEM) 15 KV was used. Further, the crystallinity and quality of the synthesized structures were characterized by a fully automatic X-ray diffractometer ($\lambda = 1.54$ nm, D/Max = 2200) using a Philips diffractometer with Cu$K\alpha 1$ radiation with an incident angle of 5°. Moreover, Raman spectroscopy was utilized to study the composition of structure. Transmission Electron Microscopy (TEM) images disclosed constrictions clusters in structure.

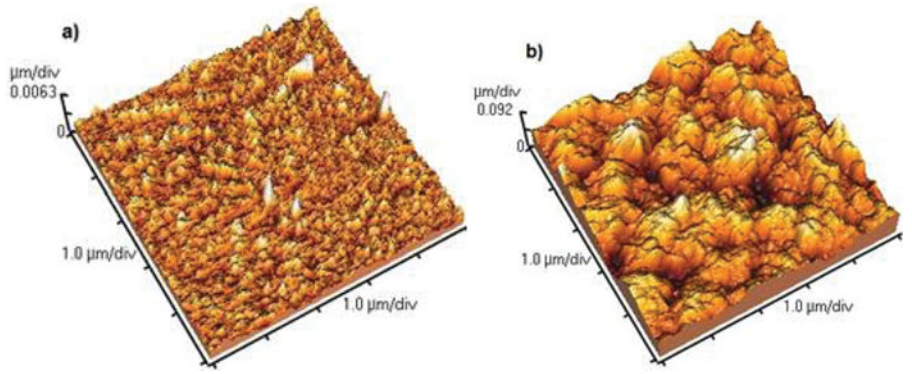

Figure 3. The AFM image of the silicon substrate coated with Fe (a) before etching and (b) after etching by H_2 gas.

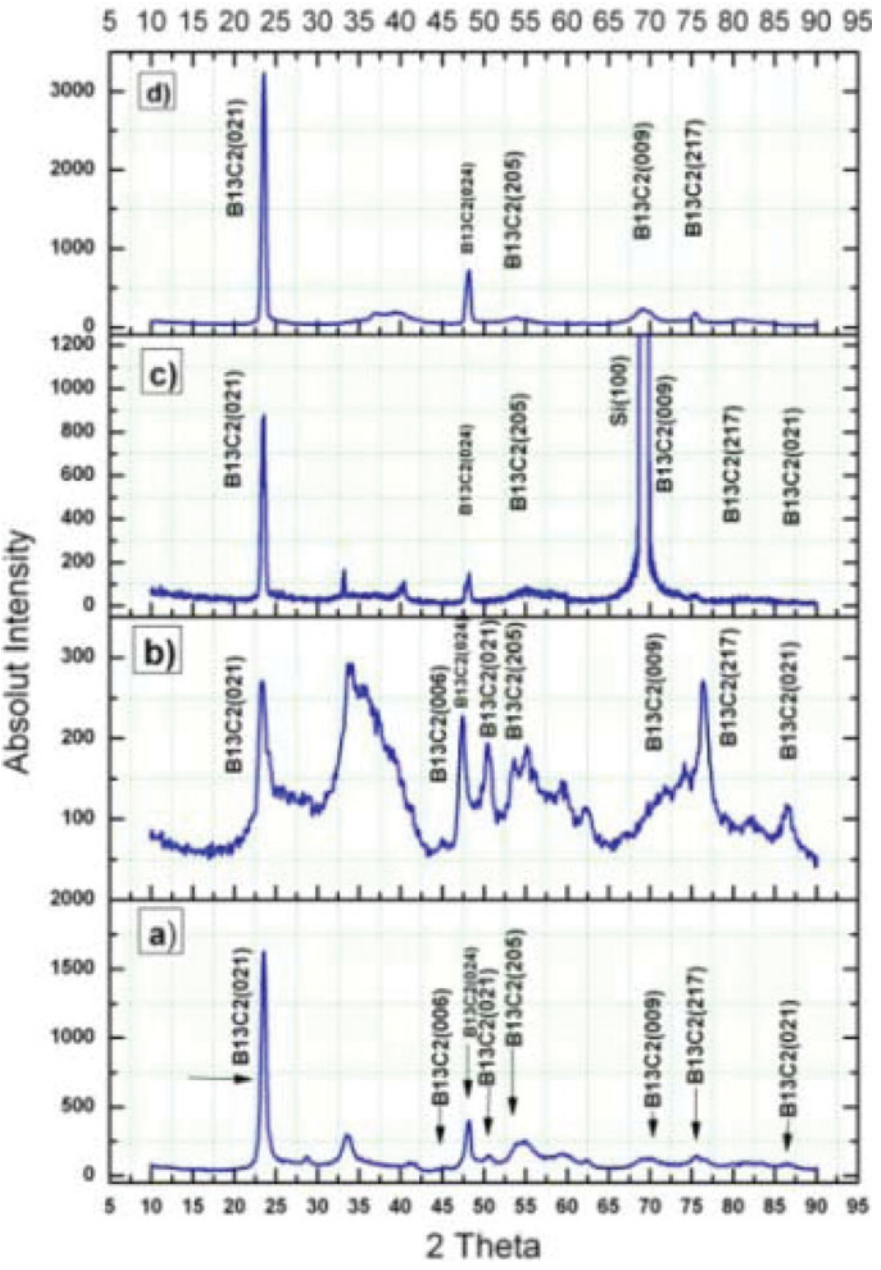

Figure 4. XRD patterns of B-doped DLC films with different contents of boron: 0.00625, 0.0125, 0.025, and 0.05 molar from a–d, respectively. In (c) profile was removed silicon (100) peak.

3. Results and Discussion

Figure 4 shows the XRD patterns of the B-doped DLC films. All XRD peaks at 23.60°, 40.32°, 48.25°, 53.40°, 75.43°, and 80.55° originated from $B_{13}C_2$ relevant to standard card and the peak at 69.17° arose from the silicon substrate. According to XRD results, the

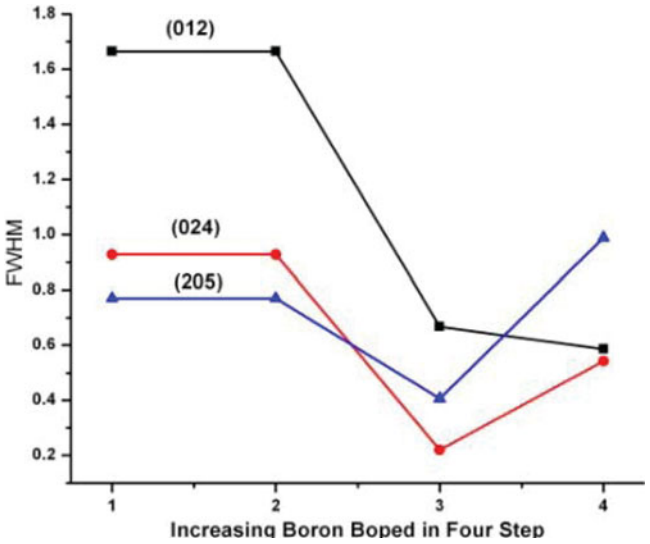

Figure 5. FWHM of peaks (012), (024), and (205) in icosahedral boron carbide.

average crystal size of nanocrystals was between 5 and 80 nm that has been calculated by Debye–Scherr formula.

$$D = 0.9 \times \lambda/(\beta \text{Cos}\, \beta), \tag{1}$$

where D = thickness of crystallite, K = constant dependent on crystallite shape 0.9, λ = X-ray wavelength, β = FWHM, and θ_β = Bragg angle. An effect of the finite crystallite sizes is seen as a broadening of the peaks in an X-ray diffraction as is explained by the Equation (1). The XRD patterns of the $B_{13}C_2$ icosahedral boron Carbide film is dominated by the peaks at 23.60°, 48.25°, and 53.40° corresponding to planes (0 1 2), (0 2 4), and (2 0 5) of boron carbide icosahedral, diffraction peaks evidence the presence of crystalline $B_{13}C_2$. FWHM had been similar treatment; see Fig. 5.

$$\text{By using } \delta = 1/D^2, \tag{2}$$

where δ = liner dislocation, D = thickness of crystallite and Stokes and Wilson formula

$$\varepsilon = \beta/4 \ \tan\ \theta_\beta, \tag{3}$$

θ_β = Bragg angle, β = FWHM; see Table 1, by increasing level doping decreased dislocations in layers and tension also layers was better constructed. Also, numbers of crystals per unit area:

$$N = t/D^3, \tag{4}$$

where t = thickness film, D = thickness of crystallite boron carbide icosahedral.

4. The Raman Spectrum of Boron-Doped DLC

Raman spectroscopy is regarded as a widespread, nondestructive technique for characterizing various carbon structures [16] and has been extensively used for $B_{13}C_2$ characterization

Table 1. Peak with highest intensity signifying

Sample	FWHM (0 1 2)	Crystal size (nm)	FWHM (0 2 4)	Crystal size (nm)	FWHM (2 0 5)	Crystal size (nm)	c/a	N.10^{19} (L^{-2})	$\delta.10^{15}$ (Line/m^2)	$\varepsilon.10^{-3}$ (Lin^{-2}/m^{-2})
(a)	0.7147	1.89	0.7436	2.04	0.8498	1.82	1.044465962	1.728024042	8.26446281	2.99332617
(b)	1.6642	0.85	0.9277	1.63	0.7702	2.01	1.044465983	35.9	40	5.754393988
(c)	0.6676	2.12	0.2202	6.89	0.4066	3.81	2.335496874	1.331088519	6.944444444	2.7933653593
(d)	0.5861	3.48	0.5427	2.79	0.9885	1.40	2.335492276	0.8381924198	5.102040816	2.538628893

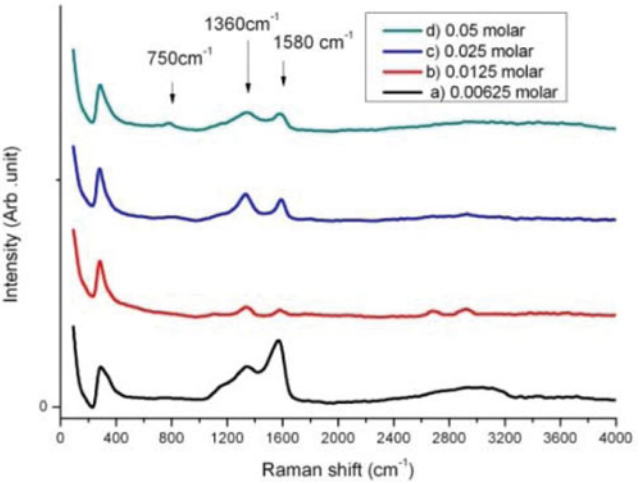

Figure 6. Raman spectra from samples shows evolutions in positions, intensity, and FWHM of peaks from (a) 0.00625, (b) 0.0125, (c) 0.025, and (d) 0.05 molar boron doped in DLC films.

[17, 18]. Being able to discriminate between sp^2 and sp^3 carbon sites, it is the most commonplace method utilized for corroborating the quality of crystalline films. Therefore, by using Raman spectroscopy, it is straightforward to distinguish involvements of $B_{13}C_2$ from the modes of the aromatic sp^2 clusters observed at higher frequencies. However, the roots of some $B_{13}C_2$ peaks are still debatable. One of the $B_{13}C_2$ modes is found around $275-325\ cm^{-1}$. The other $B_{13}C_2$ modes at 650–1000 cm^{-1} also put the same scaling characteristic on view. In addition to information about the boron carbide phase, substantial insight into the presence of free carbon in $B_{13}C_2$ can also be obtained by careful Raman analysis [17]. By adroitly analyzing Raman results, one is able to attain significant knowledge concerning the existence of free carbon in $B_{13}C_2$ as well as figuring out the boron Carbide phase. The first-order Raman spectrum of graphitic single crystals is only peaked at 1589 cm^{-1} (G-peak), which is the fingerprint of stretching vibrations of double, C=C, bonds. In the presence of graphitic domains of finite size, amorphization of the graphene layer, or defects, a second peak emerges at $1300-1360\ cm^{-1}$ (D-peak) which can be assigned to breathing vibrations of aromatic sixfold rings in finite graphitic domains. At visible or near infrared excitation wavelength, λ, the diameter, L, of the sp^2 domain has peculiarly shown to affect the I_D/I_G ratio [17, 18]. The whole selection rules can be disregarded while at a higher degree of disorder, and the total density of phonons can be observed. Particularly, at 1350 and 1580 cm^{-1}, phonons can be observed illustrating the existence of microcrystalline graphite and the scattering intensity in the 1400–1600 cm^{-1} region will be due to non-diamond-carbon impurities [19, 20]. As indicated in Fig. 6, peaks at 280 cm^{-1}, 750 cm^{-1}, 1340 cm^{-1}, and 1580 cm^{-1} were detected in Raman spectra. The peaks appeared at 280 and 750 cm^{-1} are associated with boron carbide icosahedral. Despite the frequent appearance of Raman peaks in the 250–350 cm^{-1} region in $B_{13}C_2$ ceramics, a good knowledge of their origin has not yet been acquired [21–23]. The peak at $\sim$750 cm^{-1} is related to icosahedral mode which is not sensitive to annealing, in agreement with infrared spectroscopy results. No sign of graphitic inclusions was observed [24]. The peaks centered at 1349 and 1580 cm^{-1}, are known as *D* and *G* bands, respectively. Owing to the restricted dimensions of the crystallites, a slight breaking of the selection rules may occur and the

Table 2. Summarize data Raman

Sample	280 bond (cm^{-1})	Intensity	FWHM (cm^{-1})	750 bond (cm^{-1})	Intensity	FWHM (cm^{-1})	D-bond (cm^{-1})	Intensity	FWHM (cm^{-1})	G-bond (cm^{-1})	Intensity	FWHM (cm^{-1})	I_D/I_G	L_a(nm)
(a)	314	1,744	88.44	775	395	97.5	1,361.5	1,758	370	1,539	2,901	170	0.60	73
(b)	287.5	2,533	48	777	265	215	1,333.6	530	94	1,584	400	81	1.32	58.3
(c)	286.7	2,300	52.5	775	184	1,856	1,328	1,197	118	1,581	965	89.6	1.24	35.48
(d)	298.6	2315	79	779	640	128	1,339.9	1,103	255	1,551.8	1,051	322	1.04	41.94

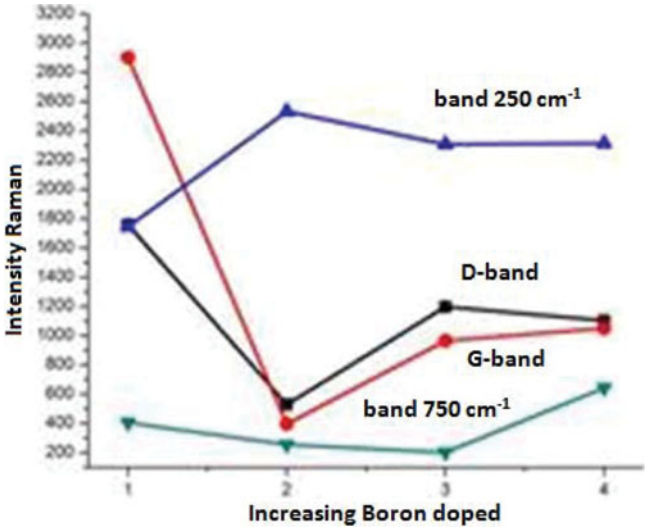

Figure 7. Profile of variation in intensity four bands 280 cm^{-1}, 750 cm^{-1}, D band, and G band at Raman spectrum by increasing boron doped.

phonons located adjacent to the center of Brillouin zone scatter the incident photons. At a greater level of disorder, all of the selection rules can be 11 broken, and the total density of phonons can be observed. The G peak exhibits region center phonons of E_{2g} symmetry and D peak reveals K-point phonons of A_{1g} symmetry of graphite [25, 26]. Sharp *G* and *D* peaks observed around 1573 and 1340 cm^{-1} suggest the presence of some species such as monocrystalline graphite in the films. The formation of sp^2 hybridized aromatic *C* rings and localized amorphization in $B_{13}C_2$ can be evidently deduced from the development of these peaks for all types of samples. Further, a higher level of structural damage or amorphization in $B_{13}C_2$ is concluded when more intense G and D peaks are obtained by doping boron [27–32]. In Table 2 G-peak FWHM, (I_D/I_G) and in Fig. 8 the G and D peak positions, as a function of the chemical composition of the films are illustrated. By comparing the data measured from the DLC films [7, 15, 20] with those from B-DLC films, it can be seen that incorporation of B into DLC films brings on the concurrent transfer of both G and D peak positions towards lower Raman frequencies which signifies the evolution of sp^3 fourfold coordinate bonding in the amorphous carbon films. Moreover, Fig. 7 shows that by increasing content B-alloyed DLC film has an intensity decrease of G-band and D-band and 750 cm^{-1} band and then increase the intensity. The broadening of the G-band relies on the increase of mass density and hardness of DLC films that it had result of added boron to films. The size of the graphite crystallites is inversely proportional to the I_D/I_G ratio, in other words, $I_D/I_G = C/La$, where La is the sp^2 correlation length or in-plane crystallite size. The broadening of G-band along with the simultaneous decrease of I_D/I_G, accompanied by the coexistent downshift in both *G* and *D* peaks, as shown in Table 2, could lead us to the conclusion that incorporating B into DLC films facilitates the formation of a film with a boosted sp^3 bonding structure Moreover, the decrease observed in the intensity of *G* and *D* peaks stem from disrupting the vibrational behavior of the film and diminution of polarizability in the molecules of the lattice. The decrease of polarizability the promotion of a great fraction of δ bonds between B—C atoms [15, 33, 34]. According to Fig. 8, the

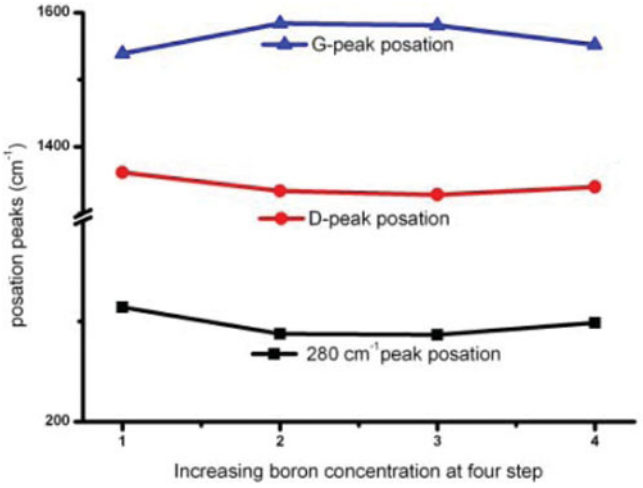

Figure 8. Profile of variation in position peaks at Raman spectrum by increasing boron doped.

dispersion in G-band toward higher wavelengths due to the grain size reduction from 73 nm to 42 nm and the subsequent phonon confinement which induces phonons away from Γ to be involved with $q = 1/\mathrm{La}$. According to Tuinstra–Koenig formula (Eq. 5), La decreases with the increase of the intensity of appears as a result of defects in the structure [35] that

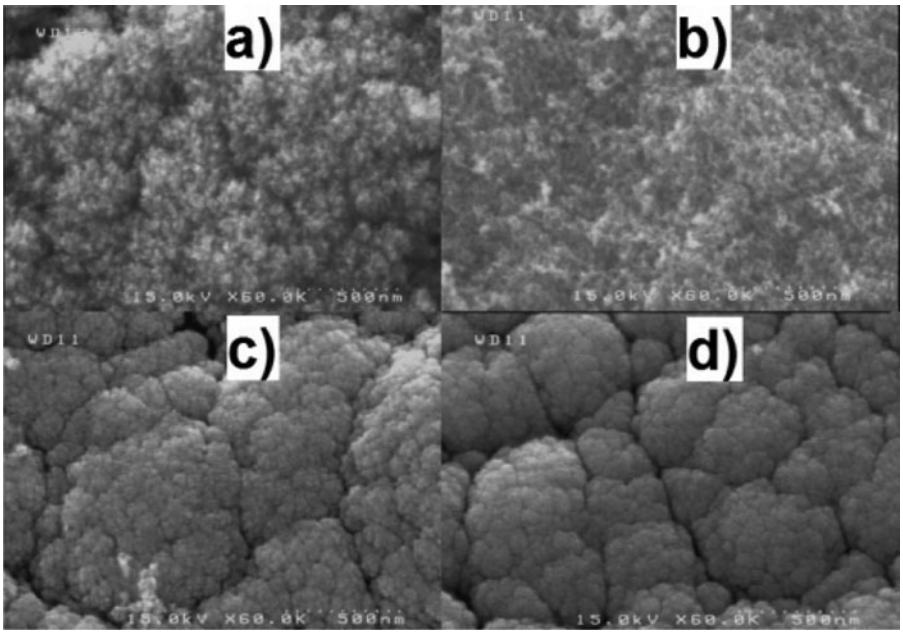

Figure 9. FE-SEM images show boron doped DLC films in different contents (a) 0.00625, (b) 0.0125, (c) 0.025, and (d) 0.05 molar. Visible by increase of cracks on surface of the structure in Figs. 6(a), (c), and (d) are relatively to doped boron in the grown film.

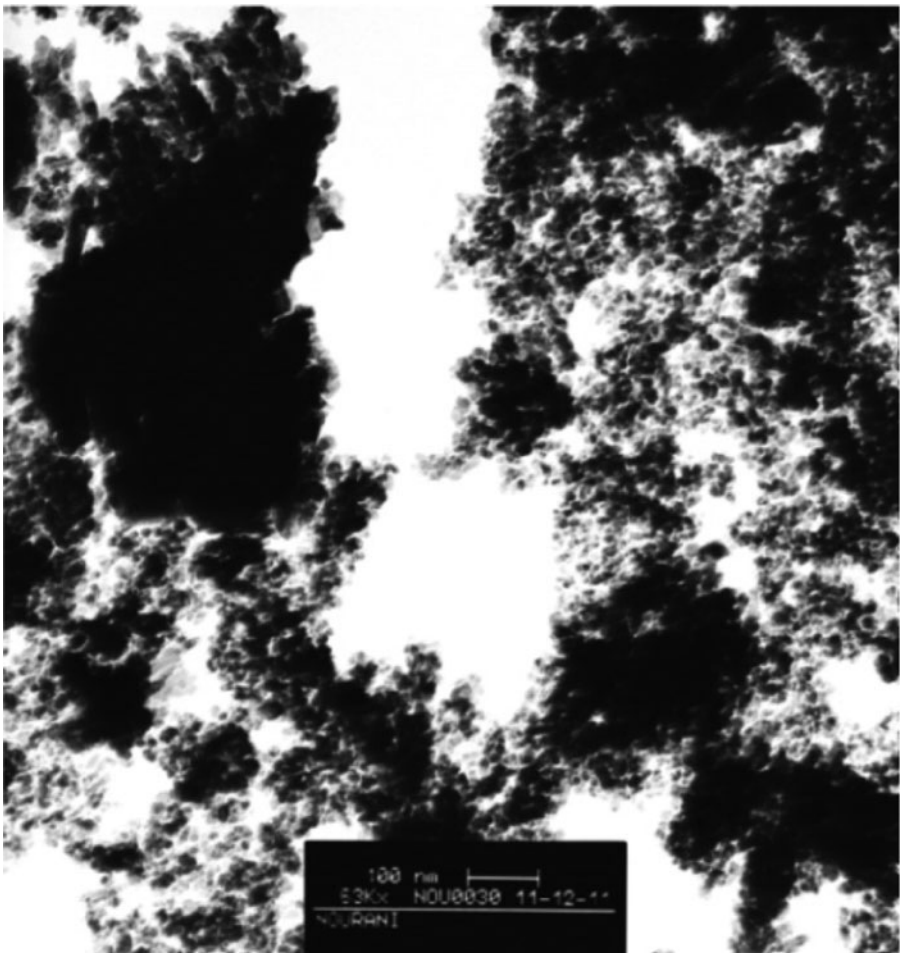

Figure 10. TEM image shows boron doped DLC films in contents (a) 0.00625 molar, Samples were prepared by dispersing the powder products in n-hexane by ultrasonic treatment, dropping the mixture onto a porous carbon film supported on a copper grid and then drying the film in air. With the aid of Microstructure Measurement software, TEM images illustrate that the size of produced clusters is average 22 nm.

surely it was result of doped boron. Tuinstra–Koenig formula is:

$$I_G/I_D = c/La \tag{5}$$

Figure 9 shows the FE-SEM images of B-doped DLC films. The FE-SEM results indicate that the cracks exist all over the surface and relatively increase by raising the amount of dopant. In Fig. 9(a), it can be seen that, there are low cracks and shallow and the crack paths are not straight on the surface. On the other hand, Figs. 9(a) and (d), show that the surface of the coated film has particle-like features with less than 1 micrometer in diameter. Small, nonregularly shaped surface voids are also detected. For samples in Fig. 9(d), the congeries is very different from that in Fig. 9(a). In Fig. 9(d),

the multiplicity of cracks on the film surface is noticeable compared to those observed in Fig. 9(a). On the other hand, the specimen microstructure in Fig. 9(b) differs very much from that of the other specimens. Increase of cracks on surface of the structure in Figs. 9(a), (c), and (d) was grown by doped boron in the film. Measurements indicate that the size of agglomerations on the surface for sample (a) is less than 1 μm and for samples (c) and (d) is less than 0.5 μm. These agglomeration phenomena on the structure surface due to the increase of doping dosage which then leads to the upsurge of cracks. It may be inferred according to the depth of cracks that agglomeration triggers from the moment growth initiates and gradually escalates as the growth time goes up and brings about more cracks on the surface. Also, in the Fig. 10 TEM image shows boron doped DLC films in contents (a) 0.00625 molar, samples were prepared by dispersing the powder products in *n*-hexane by ultrasonic treatment, dropping the mixture onto a porous carbon film supported on a copper grid and then drying the film in air. With the aid of Microstructure Measurement software, TEM images illustrate that the size of produced clusters is average 22 nm.

The spacing's were measured over different regions in the micrograph and then averaged, and results for three sample are congeries size was below 1 μm for (a) below 0.5 μm for (c) and (d) samples [36].

5. Conclusion

According to XRD patterns, SEM images and Raman spectra, the structure of the film was determined as DLC along with grown boron carbide icosahedrals ($B_{13}C_2$) in its texture. The size of these icosahedrals calculated by Debye–Scherrer's equation was between 5 nm and 80 nm. Further, the grain size has been estimated between 42 nm and 73 nm on the basis of Raman peaks using Tuinstra–Koenig formula. Raman spectroscopy demonstrates variations in D and G peaks which are attributable to the presence of localized amorphization in $B_{13}C_2$. Additionally, the shift in G peak location towards higher wavelengths stems from the fact that owing to the diminution of grain size, phonon confinement provokes phonons to be away from $\mathbf{\Gamma}$ and contribute with $q = 1/L_a$. Also, L_a factor reduces with increasing doping amount from 73 nm to 42 nm. The high intensity of G-band and the low intensity of D-band in Raman spectrum in Fig. 6 black line exhibit the high degree of graphitization in matrix which increases to $I_D/I_G = 1.3$ upon raising the amount of boron incorporation in the matrix and the formation of sp^3 hybrid in the film. With further increasing the amount of boron alloy, a balance will be set between sp^2 and sp^3 hybrids in the film and the I_D/I_G ratio decreases to 1. This occurs as a result of the substitution of boron atoms with carbon atoms and the development of B−C bond. Moreover, the decrease observed in the intensity of G and D peaks stem from disrupting the vibrational behavior of the film and diminution of polarizability in the molecules of the lattice. One of the factors inducing the decrease of polarizability is the promotion of a great fraction of δ bonds between B−C atoms. The entire sp^2 sites lead to the formation of G peak. However, D peak attributes to sixfold rings. Hence, the decrease of number of rings per cluster and the increase of the fraction of chain groups gives rise to the reduction of I_D/I_G ratio. Surface morphology in SEM results discloses the growth of cauliflower structures. It is deduced that the increase of doping amount leads to creation of deep cracks on the surface and incites the reduction of the dimensions of agglomerations. Moreover, it causes damages to its uniformity which decreases with increasing doping boron from 1 to 0.5 μm.

References

[1] Ma, Z. Q., & Liu, B. X. (2001). *Sol. Energ. Mat. Sol. C.*, *69*, 339.
[2] Nekkanty, S., & Walter, M. E. (2004). *Surf. Coat. Technol.*, *183*, 1.
[3] Ullah, M., & Ahmed, E. (2012). *Curr. Appl. Phys.*, *12*, 945.
[4] Wang, F. M., Chen, M. W., & Lai, Q. B. (2010). *Thin Solid Films*, *518*, 3332.
[5] Kautek, W., Pentzine, S., Conradi, A., Kruger, J., & Brzeinka, K.-W. (1996). *Appl. Surf. Sci.*, *106*, 158.
[6] Conde, O., Silvestre, A. J., & Oliveira, J. C. (2000). *Surf. Coat. Technol.*, *125*, 1411.
[7] He, X.-M., Walter, K. C., & Nastasi, M. (2000). *J. Phys. Cond. Matter*, *12*(8), L183–L189.
[8] May, P. W. *et al.* (2008). *Diamond Relat. Mater.*, *17*, 105.
[9] Monteiro, O. R., Delplancke-Ogletree, M.-P., & Klepper, C. C. (2003). *J. Mater. Sci.*, *38*, 3117.
[10] Lee, K.-W., & Harris, S. J. (1998). *Diamond Relat. Mater.*, *7*, 1539.
[11] Sezer, A. O., & Brand, J. I. (2001). *Mater. Sci. Eng.*, *B 79*, 191.
[12] Lin, C.-M., Tsai, H.-L., & Yang, C. (2012). *Surf. Coat. Technol.*, *206*, 2673.
[13] Gharam, A. A., Lukitsch, M. J., Balogh, M. P., & Alpas, A. T. (2010). *Thin Solid Films*, *519*, 1611.
[14] Eckardta, T. *et al.* (2000). *Surf. Coat. Technol.*, *126*, 6975.
[15] Pu, J.-C., Wang, S.-F., Lin, C.-L., & Sung, J. C. (2010). *Thin Solid Films*, *519*, 521.
[16] Ferrari, A. C., & Robertson, J. (2004). *R. Soc.*, *10*, 1098.
[17] Fanchini, G., McCauley, J. W., & Chhowalla, M. (2006). *Phys. Rev. Lett.*, *97*, 035502.
[18] Vast, N., Lazzari, R., Besson, J. M., Baroni, S., & Dal Corso, A. (2000). *Comput. Mater. Sci.*, *17*, 127.
[19] Kostic, R. *et al.* (2009). *Acta Phys. Pol.*, *A, 116*(1), 65–67.
[20] Ferrari, A. C. (2007). *Solid State Commun.*, *143*, 47.
[21] Ghosh, D., Subhasha, G., Lee, C. H., & Yap, Y. K. (2007). *Appl. Phys. Lett.*, *91*, 061910.
[22] Hosoi, S. *et al.* (2007). *J. Phys. Soc. Japan*, *76*, 044602.
[23] Werheit, H. *et al.* (2009). *J. Phys: Condens. Matter*, (in press).
[24] Jacobsohn, L. G. *et al.* (2004). *Appl. Phys. Lett.*, UCRL-JRNL-201802.
[25] Baroni, N. V. S. *et al.* (1997). *Phys. Rev. Lett.*, *78*, 693.
[26] Lazzari, R., Vast, N., Besson, J. M., Baroni, S., & Corso, A. D. (1999). *Phys. Rev. Lett.*, *83*, 3230.
[27] Tuinstra, F., & Koenig, J. L. (1970). *J. Chem. Phys. 53*, 1126.
[28] Al-Jishi, R., & Dresselhaus, G. (1982). *Phys. Rev. B*, *26*, 4514.
[29] Ager III, J. W., Walukiewicz, W., McCluskey, M., Plano, M. A., & Landstrassb, M. I. (1995). *Appl. Phys. Lett.*, *66*(5).
[30] Parthasarathy, G., Sreedhar, B., & Chetty, T. R. K. (2006). *Curr. Sci.*, *90*(7).
[31] Azevedo, A. F., Baldan, M. R., & Ferreira, N. G. (2012). *Int. J. Electrochem.*, *2012*, 508453, 16.
[32] Watanabe, T. *et al. Diamond Relat. Mater*.
[33] He, X.-M., Hakovirta, M., & Nastasi, M. (2004). *J. Phys.: Condens. Matter*, *16*, 8713.
[34] Wua, Y.-H., Hsua, C.-M., Chiab, C.-T., Linc, I.-N., Chenag, C.-L. (2002). *Diamond Relat. Mater.*, *11*, 804.
[35] Robertson, J. (2002). *Mater. Sci. Eng.*, *37*, 129.
[36] Nekkanty, S., & Walter, M. E. (2004). *Surf. Coat. Technol.*, *183*, 1.